STK11/LKB1 Loss of Function Is Associated with Global DNA Hypomethylation and *S*-Adenosyl-Methionine Depletion in Human Lung Adenocarcinoma

Michael J. Koenig[1], Bernice A. Agana[2], Jacob M. Kaufman[3], Michael F. Sharpnack[1], Walter Z. Wang[1], Christoph Weigel[1], Fabio C.P. Navarro[4,5], Joseph M. Amann[1], Nicole Cacciato[1], Rajeswara Rao Arasada[1], Mark B. Gerstein[4,5,6], Vicki H. Wysocki[2], Christopher Oakes[1], and David P. Carbone[1]

ABSTRACT

STK11 (liver kinase B1, LKB1) is the fourth most frequently mutated gene in lung adenocarcinoma, with loss of function observed in up to 30% of all cases. Our previous work identified a 16-gene signature for LKB1 loss of function through mutational and nonmutational mechanisms. In this study, we applied this genetic signature to The Cancer Genome Atlas (TCGA) lung adenocarcinoma samples and discovered a novel association between LKB1 loss and widespread DNA demethylation. LKB1-deficient tumors showed depletion of *S*-adenosyl-methionine (SAM-e), which is the primary substrate for DNMT1 activity. Lower methylation following LKB1 loss involved repetitive elements (RE) and altered RE transcription, as well as decreased sensitivity to azacytidine. Demethylated CpGs were enriched for FOXA family consensus binding sites, and nuclear expression, localization, and turnover of FOXA was dependent upon LKB1. Overall, these findings demonstrate that a large number of lung adenocarcinomas exhibit global hypomethylation driven by LKB1 loss, which has implications for both epigenetic therapy and immunotherapy in these cancers.

Significance: Lung adenocarcinomas with LKB1 loss demonstrate global genomic hypomethylation associated with depletion of SAM-e, reduced expression of DNMT1, and increased transcription of repetitive elements.

Lung adenocarcinomas with LKB1 loss display genomic hypomethylation associated with depletion of *S*-adenosyl-methionine, reduced expression of DNMT1, increased repetitive element transcription, and resistance to azacytidine.
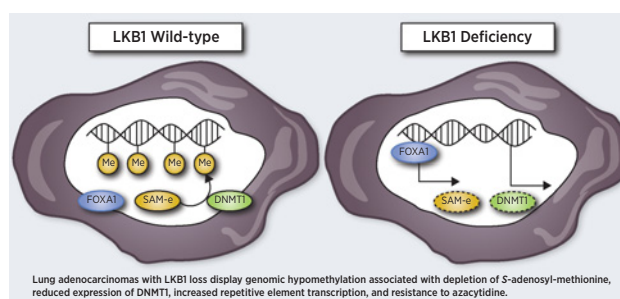
Introduction

LKB1 is a serine-threonine kinase responsible for regulation of cell polarity and the AMPK signaling pathway (1–5). LKB1 loss of function is common in primary lung adenocarcinomas (6–8). LKB1 mutation cooccurs somewhat more frequently with oncogenic KRAS mutations, but can occur independently of KRAS mutation as well. Through AMPK and the AMPK-like kinases, LKB1 exerts control over cell metabolism, polarity, and morphology (9–11). More recent studies have found an association of LKB1 loss with resistance to immuno-therapy (12, 13). Previous work by our group showed that a functional genetic classifier for LKB1 loss of function (which will from now on be referred to as "LKB1 loss") was able to robustly categorize patients with bona fide LKB1 mutations as well as an additional subset of those with gene expression patterns similar to LKB1 mutant patients but no sequenced mutation (14).

One of the primary forms of epigenetic regulation is the methylation of CpG residues on DNA by DNA methyltransferases (DNMT refs. 15, 16). There are three DNMTS: DNMT1, DNMT3a, and DNMT3b. DNMT1 preferentially acts on hemimethylated DNA during DNA replication, passing on CpG patterns to daughter cells, while DNMT3a and DNMT3b act independently of DNA replication and can methylate CpGs *de novo* (17, 18). An essential substrate for DNMT-mediated methyl group transfer is *S*-adenosyl methionine (SAM-e; refs. 19–21) and the maintenance of CpG methylation by DNMT1 is dependent on continued regeneration of SAM-e. While SAM-e is a substrate for many methyltransferases, it has been shown that its depletion *in vitro* can directly result in global CpG demethylation. Inhibition of DNMT1 activity by azacytidine, a nucleoside analogue that binds irreversibly to DNMT, induces broad CpG hypomethylation in both normal and cancer cells (22).

A murine pancreatic cancer model recently showed that LKB1 loss with concurrent KRAS mutation drives repetitive element hypermethylation and serine biogenesis, and specifically identified increased SAM-e production in LKB1-loss tumors (21). Another recent study showed that KRAS-LKB1 comutation led to a buildup of mitochondrial dsDNA in lung cancer cell lines and depletion of the dsDNA sensor STING (23). A third study in a mouse model

of *Kras*-driven lung adenocarcinoma that *Lkb1*-mutation is associated with loss of polycomb repression and H3K27 trimethylation and squamous transdifferentiation (24). These studies complemented the existing observation from The Cancer Genome Atlas (TCGA) that identified a pattern of hypermethylation in KRAS-mutant lung cancers known as the CpG island hypermethylation phenotype (CIMP), in which regions of chromatin normally repressed by the polycomb repressor complex instead undergo repression by CpG hypermethylation (8). CpG methylation and H3K9 trimethylation is another mode of chromatin silencing, and is especially common in repression of repetitive elements.

DNMTs maintain CpG methylation at noncoding DNA and demethylation of repetitive elements can lead to their transcription into dsRNA. dsRNAs produced by endogenous retroviral elements (hERV) or transcription of repetitive elements can produce an innate immune response similar to that produced by viral infection, and this can be triggered by azacytidine (25). The demethylation of cryptic transcriptional start sites and production of dsRNAs leads to TLR3 activation in cancer cells and is a mechanism of DNMTi toxicity (26, 27)

In this article, we further studied the role of LKB1 loss of function in human lung adenocarcinoma, and its impact on epigenetics alone or in conjunction with KRAS mutation.

Materials and Methods

TCGA data analysis

Using the LKB1-loss signature (14), LKB1-wild-type (WT) and LKB1-loss tumors were identified in the TCGA lung adenocarcinoma (LUAD) provisional dataset. Tumors were assigned to the LKB1-WT group if the signature identified them as WT, had no LKB1 copy number alterations, and no LKB1 mutations by DNA sequencing; tumors were assigned to the LKB1-loss group if they were identified as loss by signature, had known copy number loss, or had sequenced LKB1 mutations. Methylation in this dataset was assessed using level 3 Illumina 450k methylation array data downloaded from Broad Firehose (gdac.broadinstitute.org). At the time of data download, 427 primary tumor samples and 32 matched normal adjacent tissue samples were identified with both RNA sequencing (RNA-seq) and Illumina 450k data. The sample IDs and LKB1 signature assignments are available in Supplementary Tables S1 and S2. Differential methylation analysis and clustering was performed in R and Qlucore Omics Explorer (Qlucore). Pairwise comparisons of average β-value between groups was made using two-tailed two-sample Student *t* test with Benjamini–Hochberg multiple comparison correction where indicated. In R, processed level 3 β-values were converted to M-values as described in the literature (28). Differentially methylated loci were determined from M-values using the lmfit and eBayes functions in the limma package as described in the literature (29). Heatmap figures of top differentially methylated loci were generated using the original level 3 β-values. Alignment of hypomethylated loci to RepeatMasker was made using the homo sapiens repeat library open-4.0.5 (repeatmasker.org).

Cancer Cell Line Encyclopedia data analysis

Preprocessed Reduced-Representation Bisulfite Sequencing (RRBS) data from cancer cell lines was downloaded from the Cancer Cell Line Encyclopedia (CCLE; https://portals.broadinstitute.org/ccle/data). Ninety-eight non–small cell lung cancer (NSCLC) cell lines were identified. Using the LKB1 loss signature (14) cell lines were assigned to the LKB1-WT group if the signature identified them as WT and they

harbored no LKB1 mutations by DNA sequencing; tumors were assigned to the LKB1-loss group if they were identified as loss by signature or had sequenced LKB1 mutations. Processed β-values from CpG islands, enhancers, and flanking transcription start sites were merged for analysis. As described above, β-values were converted to M-values and differentially methylated loci were identified using the lmfit and eBayes functions in the limma package in R. Heatmap figures of top differentially methylated loci were generated using the original β-values.

Transcription factor binding site motif enrichment

Putative transcription factor binding sites were identified using the available datasets from published chromatin immunoprecipitation sequencing (ChIP-seq) studies in the HOMER database (30). The loci of the top 5000 hypomethylated sites in LKB1-loss LUAD TCGA tumors were identified as described above. The sequence upstream and downstream by 100 bp of the hypomethylated CpG was extracted and merged to create a foreground that was tested for motif enrichment versus a sequence background matched for sequence length, CpG density, and GC content. *De novo* motifs were matched against a database of >300 motifs (http://homer.ucsd.edu/homer/motif/motifDatabase.html). The most significant enriched results from this comparison were shown in **Table 1**. Extended results are available in Supplementary Table S3.

TeXP analysis of TCGA LUAD for LINE1 expression

TCGA LUAD samples with LKB1-status characterization as described in Supplementary Table S1 were used to assess *LINE1* (*L1Hs*) expression. TeXP was designed to characterize repetitive element transcription using typical RNA-seq data while accounting for pervasive transcription and multiple transcripts of repetitive elements (31). In brief, the majority of RNA-seq reads overlapping LINE1 elements are derived from pervasive transcription of a subset of those elements. TeXP uses mappability signatures from the autonomous transcription of pervasive and simulated LINE1 subfamilies to deconvolute reads overlapping LINE1 elements. It then counts the reads overlapping LINE-1 subfamilies and calculates the best combination of signatures that explains the observed read counts. TeXP-derived *LINE1* RPKM values for TCGA LUAD samples were compared using a Wilcoxon rank-sum test with continuity correction

Human cell lines and LKB1 constructs

All human cell lines were acquired from ATCC. *Mycoplasma* testing was performed at monthly intervals on all cells in culture using the MycoAlert Plus kit (Lonza, catalog no. LT07–710); cell lines were authenticated using ATCC's Human STR service. Cells were grown on RPMI supplemented with 10% FBS and Gibco Antibiotic-Antimycotic (100X). LKB1-loss cell lines were identified using the CCLE. LKB1-loss cell lines were infected with a retroviral LKB1 construct as described previously (14, 32), and stable expression of LKB1 was confirmed by Western blot for LKB1 and p-AMPK. LKB1-WT cell lines were transfected with px459 (33) containing a guide RNA (gRNA) targeting exon 1 of LKB1 according to the protocol at crispr.mit.edu. gRNAs were identified using crispr.mit.edu, and the following three gRNA templates and their complements were used: CACCGAGCTTG-GCCCGCTTGCGGCG, CACCGGTTGCGAAGGATCCCCAACG, CACCGTTCAACTACTGAGGAGGTTA. Comparison in knockout efficacy between the three gRNAs showed that gRNA #2 was superior, and it was used for all subsequent experiments. Transfected cells were cloned by dilution in 96-well trays, and LKB1-loss was confirmed by Western blot and Sanger Sequencing of the

targeted exon. WT clones were selected from cells transfected with px459 containing no gRNA.

For LKB1 overexpression in A549 and H23 cells, empty pBABE viral plasmids, pBABE-LKB1, and pBABE-LKB1-K78I, were obtained from Addgene. 293FT cells (Thermo Fisher) were transfected with viral plasmids and retroviral particles were harvested from media supernatant 48 hours after transfection. Viruses were added to target cells with polybrene, and selection with 1 μg/mL puromycin was begun 48 to 72 hours after infection. Cells were selected under puromycin for 1 to 2 weeks before performing subsequent experiments.

Western blots and cell fractionation

Whole cell protein lysates were prepared using RIPA buffer with cOmplete mini protease inhibitor and PhosSTOP (Sigma). Protein concentrations were assayed using the pierce BCA assay (Thermo-Fisher). Normalized protein was suspended in SDS loading buffer with DTT and separated by size on Criterion TGX gels 4%–15% SDS-PAGE gels (BioRad). Proteins were transferred onto polyvinylidene difluoride (PVDF) membranes using the Transblot Turbo (Bio-Rad) and treated with appropriate antibodies according to the methods recommended by their manufacturer and LI-COR, then imaged on a LI-COR CLx imager. Cellular fractions were obtained using the Thermo Scientific Subcellular Protein Fractionation Kit and Western blotted as previously described.

DNA and RNA preparation

Frozen human tumor fragments were disrupted and homogenized using sterile BioMasher II homogenizers (VWR, catalog no. KT749625–0030) followed by QIAshredder (Qiagen, catalog no. 79656). Cell culture samples were prepard using the QIAshredder alone. DNA and RNA fractions were extracted from cell lines and human tissue samples using the Qiagen AllPrep kit (Qiagen, catalog no. 80004) according to the manufacturer's protocol.

Immunofluorescence microscopy

Cells were grown on glass coverslips, fixed in 4% paraformaldehyde (PFA), and permeabilized in 0.1% Tween20. Coverslips were blocked in 5% normal goat serum for 1 hour and incubated with primary antibody overnight in a humidified chamber at 4°C. They were then washed with PBS and incubated with Alexa Fluor 488 secondary antibody for 1 hour. Coverslips were counterstained with DAPI and mounted on glass slides with Vectashield Hardset. All images were taken on an Olympus FV 1000 Filter Confocal System with a super-corrected 60× oil objective. Image adjustment and analysis was performed in Olympus Fluoroview software and ImageJ. Z-stacks were generated with summed intensities and an image mask was generated using an established algorithm (34). Median pixel intensity measured for each cell nucleus in the field; values from partial nuclei containing less than 60 μm of area were removed. Data was then exported to R for statistical analysis.

Drugs

DNMT inhibitor (DNMTi) azacytidine was purchased from Sigma (catalog no. A2385) and dissolved in DMSO. PI3K-Akt inhibitor GSK2126458 was purchased from SelleckChem (catalog no. S2658) and dissolved in DMSO.

Cell viability assays

Cells were diluted on 96-well plates at a density of 1×10^3 per well and grown for 48 hours in 0.2 mL RPMI with 10% FBS. After 48 hours, the media were replaced with fresh media containing 1% DMSO with the described concentration of azacytidine. Cell viability was assessed using the Alamar Blue reagent (ThermoFisher Scientific) according to the manufacturers' recommendations. Flourescent absorption was measured after 3–6 hours of incubation with the Alamar blue reagent.

Antibodies

The following antibodies were used for Western blotting and immunofluorescence (IF) microscopy: β-actin (CST 8H10D10), FOXA1 (CST D7P9B for western, CST E7E8W and Invitrogen PA5–27157 for microscopy), FOXA2 (Abcam 108422), FOXA3 (ABR PAI-813), Ac-FOXAαβγ K264/253/211 (elabioscience ENK026), H3 (CST D1H2), LKB1 (CST D6C05), C/EBPβ (Abcam 32358), HDAC2 (CST 3F3), DNMT1 (CST D63A6), GAPDH (CST D4C6R), PCNA (CST PC10).

Epityper and MassARRAY studies of repetitive element methylation and expression

RNA and DNA was purified from resected lung tumors using the All-Prep kit (Qiagen). Analysis of DNA methylation of repetitive elements was performed using EpiTYPER MassARRAY (25, 35). Genomic DNA was prepared from resected lung tumors using the All-Prep kit (Qiagen), and 1.0 μg of genomic DNA was bisulfite converated using the EZ DNA methylation kit (Zymo Research). Regions of interest were amplified from bisulfite-treated DNA by PCR using primers designed in EpiDesigner (Agena Biosciences). Matrix-assisted laser desorption/ionization- time-of-flight (MALDI-ToF) mass spectrometry was performed to quantitate CpG methylation. Data was analyzed using EpiTYPER software 1.2 (Agena Biosciences) and visualized using R package ggplot2. For primers and target CpGs see Supplementary Table S4.

Real-time PCRReal-time PCR was performed using TaqMan reagents (catalog no. 4331182, 4304437) on the ViiA 7 real-time PCR system. β-Actin (Hs01060665_g1) was used for normalization of CXCL8 (Hs00174103_m1), IRF3 (Hs01547283_m1), IRF7 (Hs01014809_g1), AHCYL1 (Hs00198312_m1), MAT2A (Hs00428515_g1), MTR (Hs01090026_m1), PSAT1 (Hs01107691_g1). Calculation of ΔC_t, $\Delta\Delta C_t$, and fold change values was performed using Graphpad Prism 8. Primer sequences are available in Supplementary Table S5.

Quantification of *LTR12* dsRNA production was accomplished as previously described using a qPCR approach (25), with minor modifications. SYBR green master mix was used (Applied Biosystems). In short, three primer pairs were used for *LTR12* transcripts (primer pairs 1–3, Supplementary Table S5). Expression signals were normalized to three house keeping gene signals (primer pairs 4–6, Supplementary Table S5). Calculation of ΔC_t, $\Delta\Delta C_t$, and fold change values was performed using Graphpad Prism 8. Data show average normalized signal of the three *LTR12* primer pairs.

Human tumor samples

Fresh frozen tissue samples were obtained from 54 patients with resected early-stage lung adenocarcinoma using the Total Cancer Care (TCC) biorepository at Ohio State University (OSU, Columbus, OH). Tumor fragment sizes ranged from 40 – 80 mg. RNA and DNA extracts were prepared as described above and analyzed by NanoString using a previously described signature for LKB1 loss (14, 32). Of the 54 patient samples, 3 had a second fragment of tumor in the biorepository that was obtained and processed. LKB1 status by NanoString signature was found to be concordant between these secondary samples, and all subsequent results from

downstream experiments were treated as biological replicates and averaged before further analysis. 17 samples were identified as LKB1 loss by a combination of NanoString signature and the OSU lung cancer pulmonary mutation panel (https://pathology.osu.edu/divisions/Clinical/molpath/tests.html). The remaining 37 were characterized as LKB1-WT.

LC/MS-MSThirty-three of the human tumor samples above were used for LC/MS-MS metabolomics. LKB1 status was determined by a similar classification scheme to that used for TCGA samples: loss signature was calculated using a custom-designed NanoString panel and combined with an in-house molecular pathology panel. 9 of the 33 samples used were classified as LKB1 loss.

Tissues were homogenized with biomasher II tissue grinder and metabolites extracted with ice-cold extraction solution (Optima LC–MS grade methanol/water/chloroform 1:1:2). Samples were placed on an orbital shaker for 30 minutes at 4°C. Insoluble proteins and lipids were pelleted by centrifugation at 4°C for 10 minutes at 2,000 × g and supernatants were collected and filtered through a 0.2-μm PTFE filter. Samples were dried under a stream of nitrogen and stored at −80°C until subsequent analysis.

For MS analysis, metabolites were reconstituted in 0.1% formic acid in a ratio of 3 μL of solvent per mg tissue. Metabolites were loaded for RP-UPLC separation on an UltiMate 3000 2D RSLCnano system and mass analyzed by a Q Exactive Plus hybrid quadrupole-orbitrap mass spectrometer. Analytical separation was achieved on a C18 reverse phase column (75 μm x 15 cm, nanoACQUITY UPLC 2.1 μm HSS T3) using 0.1% formic acid (A1) and acetonitrile with 0.1% formic acid (B1) as mobile phases in a 35-minute gradient. The heated capillary temperature and electrospray voltage on the Q Exactive Plus were 275 °C and 1.8 kV, respectively, using top 15 data dependent acquisition in positive ion mode. Three technical replicates were performed for each sample. Metabolite identifications were obtained via Progenesis QI software using the human metabolome database.

Using MetaboAnalyst, spectral intensities were log-normalized, zero values were replaced with sample-specific minimum values, and data was autoscaled. Comparison of spectral intensities from was performed using lmfit and eBayes functions in limma. Enrichment of untargeted metabolomics data from LKB1-WT compared with LKB1-loss status was performed using mummichog and mummichog2 (36).

Results

LKB1 loss associated with global demethylation

To determine the impact of LKB1 loss-of-function on epigenetic regulation in human lung cancer, we used TCGA lung adenocarcinoma Illumina 450K microarray data and tested if loss of LKB1 was associated with altered CpG methylation. We compared β-values from TCGA LUAD samples that had been classified as either LKB1-WT or LKB1 loss based on our genetic signature (14). We similarly analyzed 98 NSCLC cell lines with reduced representation bisulfite sequencing (RRBS) data available through the CCLE. We observed a significant decrease in average β-value when comparing WT tumors with L tumors and KRAS-mutant/LKB1-WT (K) tumors with KRAS-mutant/LKB1-loss (KL) tumors (**Fig. 1A**). We observed the same phenomenon in NSCLC cell lines (**Fig. 1B**). As previously described in the literature (37), cancer cell lines display decreased average β-values compared to primary human tumor samples. In total 147,731/438,380 (33.7%) of analyzed TCGA CpGs were significantly hypomethylated in LKB1 loss, while only 3,560 (0.8%)

were hypermethylated (Benjamini–Hochberg-adjusted P value cut-off 0.01). Visualizing the top 5,000 hypomethylated CpGs from TCGA samples shows a clear distinction between LKB1-loss and LKB1-WT tumors and that CpG hypomethylation in LKB1-loss tumors affects sites that are highly methylated and lowly methylated at baseline (**Fig. 1C**). A similar pattern is observed in CCLE samples (Supplementary Fig. S1A).

We tested whether overexpression of LKB1 in cell lines with LKB1 loss or CRISPR-mediated knockout of LKB1 would affect DNA methylation. We used an ELISA-based approach to directly test LINE-1 5mC concentration, which is an established surrogate measure for global DNA methylation. In a composite comparison of our cell-line models, we observed no significant changes in 5mC concentration (Supplementary Fig. S1B). This result could reflect the possibility that epigenetic changes introduced to cell lines during the culture and selection process prevent changes introduced by LKB1 loss, or perhaps that significant epigenetic changes associated with LKB1 loss require a significant amount of time manifest in a tumor.

When demethylated CpGs were compared to ENCODE histone mark ChIP-seq in normal human lung fibroblasts (NHLF) and LKB1-loss A549 cells, we observed that A549 cells show dramatic enrichment of active histone marks H3K4me3 and H3K27ac and loss of inactive histone mark H3K9me3; this was consistent with observed higher methylation in matched normal lung tissue (Supplementary Fig. S2A and S2B).

Although KRAS mutations have been associated with methylation gain in LUAD (8, 38, 39) and colorectal cancer (40), broad methylation loss in LKB1 loss lung tumors occurred regardless of KRAS status (**Fig. 1A**). To explore the potential effect of concurrent KRAS mutation, we analyzed the differences between KL and K tumors. In this comparison, hypomethylation is again LKB1-specific for many CpGs, while K tumors are similar to matched normal lung tissue (Supplementary Fig. S3A). The majority of these loci were in close proximity to transcription start-sites (Supplementary Fig. S3B and S3C). For other CpGs, K tumors display some methylation gain relative to matched normal lung tissue, however this gain is abrogated by the cooccurrence of LKB1 loss in KL tumors. Sites of K tumor–specific methylation gain are enriched for H3K27me3 marks in A549 cells, which is a signature of polycomb repression and associated with CIMP; the demethylation at these CpGs in KL tumors indicate an attenuated CIMP phenotype (Supplementary Fig. S4A and S4B). MSigDB enrichment of genes relatively hypomethylated in KL versus K tumors from TCGA confirms this hypothesis by showing polycomb-associated gene sets (Supplementary Table S6), while enrichment of KL sites hypomethylated relative to matched normal show gene sets typically associated with LKB1 loss-of-function such as glucose metabolism, LKB1-signaling, and ECM interaction (Supplementary Table S7).

LKB1-loss tumors express less DNMT1 and more of methionine sink NNMT

DNMTs maintain CpG methylation, and inhibition of DNMT1 activity by azacytidine induces hypomethylation in cancer cells (22). To determine whether DNMT expression contributes to methylation changes, we analyzed DNMT gene expression in LKB1-loss tumors. We found that LKB1 loss is associated with a concurrent decline in expression of DNMT1, the DNA methyltransferase responsible for maintenance of CpG methylation (Supplementary Fig. S5A). This suggests that loss of DMNT1 expression may contribute to the hypomethylation seen in LKB1-loss tumors. In our cell line model, LKB1 overexpression or knockout had an inconsistent effect on
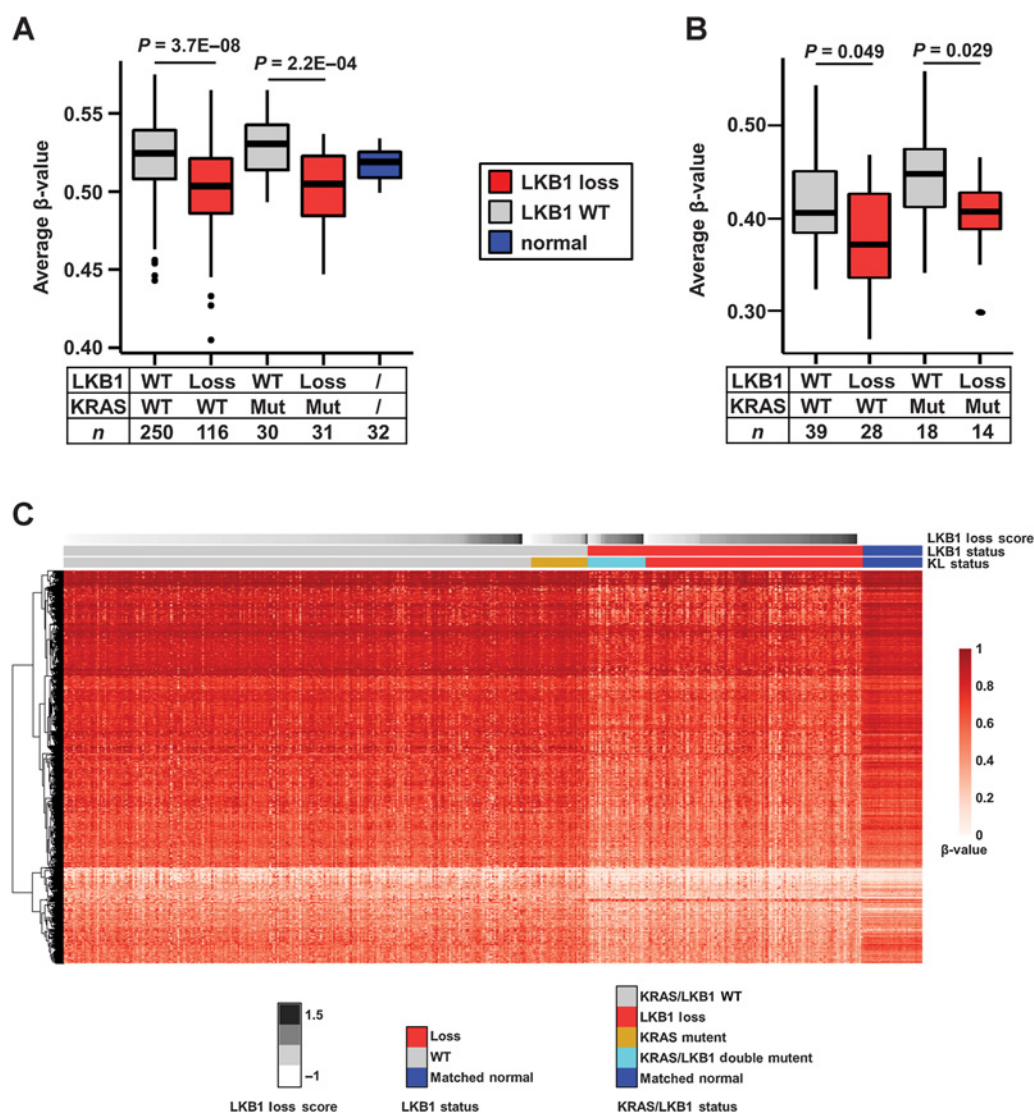
Figure 1.
LKB1 loss leads to global demethylation in patients with LUAD. β-values obtained from TCGA LUAD level 1 data. LKB1 status was determined using 16-gene classifier. **A,** Average β-values from TCGA LUAD samples with differing LKB1 and KRAS status were compared using Student *t* test to identify significant changes in average methylation based on status. LKB1-deficient tumors display significant hypomethylation compared with LKB1-WT tumors regardless of KRAS status. **B,** Average β-values from CCLE NSCLC cell lines with differing LKB1 and KRAS status were compared using Student *t* test to identify significant changes in average methylation based on status. LKB1-deficient cell lines display significant hypomethylation compared with LKB1-WT cell lines regardless of KRAS status. **C,** Clustering and heatmap visualization was performed on the top 5,000 differentially methylated probes between LKB1-loss and LKB1-WT groups. Samples were ranked by LKB1-loss signature score.

DNMT1 protein expression (Supplementary Fig. S5B–S5D). Ectopic overexpression of LKB1 in LKB1-loss A549 cells had no effect on DNMT1 expression. LKB1 knockout led to decreased mean DNMT1 expression in 2/2 Calu-1 knockout clones and decreased mean DNMT1 expression in 4/5 H358 knockout clones (this difference was not statistically significant). We also observed that TCGA LUAD tumors with LKB1 loss expressed significantly more Nicotinamide N-methyltransferase (NNMT), which is responsible for transferring methyl groups from the methionine cycle into a nicotinamide "sink" (41; Supplementary Fig. S5E). An analysis of CCLE cell lines shows that there is a significant correlation between NNMT expression and 1-methylnicotinamide levels (Supplementary Fig. S5F).

LKB1-loss tumors deplete SAM-e

The primary substrate for DNMT-mediated methyl group transfer is SAM-e (19–21) and the maintenance of CpG methylation by DNMT1 is dependent on continued regeneration of SAM-e. We hypothesized that loss of LKB1 may alter the balance of metabolic substrates for these reactions, contributing to epigenetic changes. We assessed expression of DNMT cofactor SAM-e and its related metabolites in 33 resected lung adenocarcinoma samples using untargeted LC/MS-MS (**Fig. 2A** and **B**). Enrichment of untargeted metabolomics data from LKB1-WT compared with LKB1-loss tumors using mummichog (36) showed statistically significant alterations in the methionine and cysteine metabolism pathway, with depletion of SAM-e and
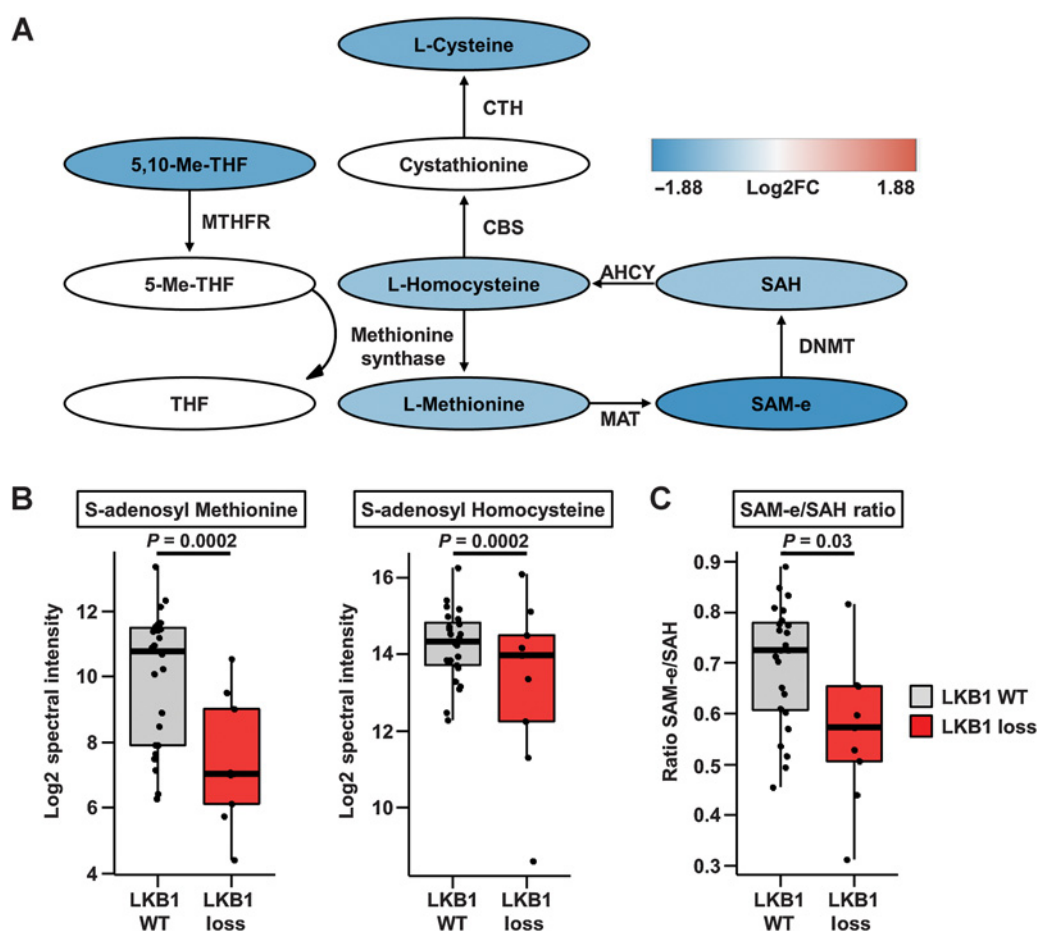
Figure 2.
Depletion of SAM-e cycle metabolites in LKB1-loss and demethylation of repetitive elements. Thirty-three resected LUAD samples were characterized for LKB1 status using a NanoString signature and were analyzed using LC/MS-MS. **A,** Untargeted LC/MS-MS of LKB1-loss patient samples indicated a significant enrichment for alterations of metabolites in the cysteine–methionine metabolic pathway; six pathway metabolites with a statistically significant decrease ($P < 0.05$) are shown in the pathway map with LogFC. **B,** Log2 fold change and Benjamini–Hochberg adjusted p-values were calculated for SAM-e and SAH using the Limma package. **C,** The ratio of SAM-e to SAH was determined using the spectral intensities from **B**. Student t test showed a statistically significant decrease in the SAM-e/SAH ratio.

related substrates in tumors with LKB1 loss (**Fig. 2A**; Supplementary Table S8). Attenuation of SAM-e precursors cysteine, homocysteine, and methionine, as well as MTHFR cofactor 5,10 methyltetrahdyrofolate was also observed in LKB1-loss tumors. Examination of spectral intensities matched with SAM-e and SAH showed a significant decline in metabolite expression as well as a significant decrease in the ratio of SAM-e to SAH in LKB1-loss tumors (**Fig. 2B** and **C**). *In vitro*, we observed that overexpression of LKB1 in previously deficient cell lines resulted in a significant decrease in *AHCYL1, MAT2A, PSAT1* expression (Supplementary Fig. S6). Taken together, this data suggests that LKB1-WT tumors have higher concentrations of SAM-e and related metabolites and concurrently have less transcription of the synthetic enzymes for the SAM-e cycle. It supports the hypothesis that LKB1-deficient tumors have reduced SAM-e availability and increased demand, while LKB1-WT tumors have more SAM-e and less demand for synthesis.

LKB1 loss demethylates repetitive elements

DNMTs maintain CpG methylation and transcriptional silencing of REs, such as *ALU, LINE*, and *LTR* elements, and DNMT inhibition induces expression from treatment-induced non-annotated transcription start sites (TINATs) in lung cancer cells (25). RE transcription and dsRNA formation contributes to the innate immune response and DNMTi sensitivity (26, 27). The demethylation of cryptic transcriptional start sites and production of dsRNAs leads to TLR3-activation in cancer cells and is a mechanism of DNMTi-induced toxicity. In the TCGA LUAD dataset we observed demethylation of REs in LKB1-loss tumors (Supplementary Fig. S7). To examine methylation of cryptic transcriptional start sites in resected LKB1-loss lung tumors, we used probes for *ALU, LINE1, LTR1*, and *LTR12* consensus CpGs. In 54 human tumors, we observed significant promoter demethylation in *LTR1, LINE1, and LTR12* CpGs (**Fig. 3A**), and a trend toward demethylation in the remaining CpGs studied (Supplementary Fig. S8). Analysis of TCGA LUAD samples using the TeXP method showed that expression of *LINE1*, specifically L1Hs, RNA was significantly higher in KL and L tumors compared to K and WT tumors, further confirming that LKB1-loss results in increased RE transcription regardless of KRAS status (**Fig. 3B**).
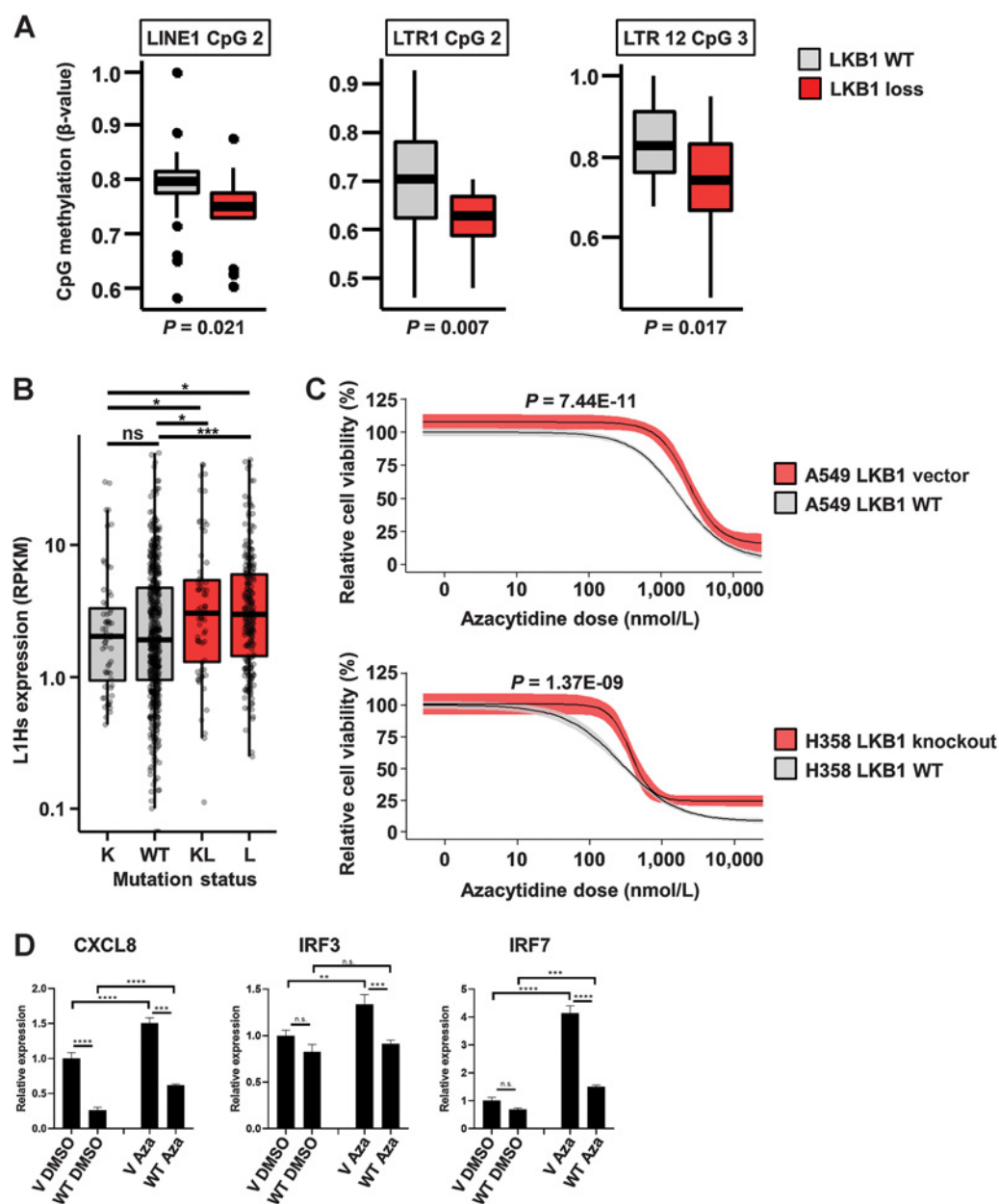
Figure 3.
LKB1 loss is associated with decreased methylation of LTR and LINE promoters, increased expression of LINE1, increased resistance to DNMT-inhibitor azacytidine, and altered interferon response to DNMT inhibition. **A,** Methylation at CpG loci repeated throughout the genome within LTRs and LINEs was assessed using Epityper, followed by MassARRAY. Comparisons were made by Wilcoxon signed-rank test with P value adjustment using the Benjamini–Hochberg method. **B,** Expression of *LINE1 (L1Hs)* repetitive elements in TCGA samples by LKB1 status was determined using the TeXP technique. Comparisons were made using a Wilcoxon rank-sum test with continuity correction ($P = 0.85$ for K vs. WT, $P = 0.018$ for KL vs. WT, $P = 0.00089$ for L vs. WT, $P = 0.028$ for KL vs. K, $P = 0.015$ for L vs. K). **C,** LKB1-deficient A549 cells transfected with pBABE empty vector (V) or pBABE-LKB1 (WT) were treated with azacytidine for 7 days; viability data at the end of the experiment was fitted to a log-logistic model using the *drc* package in R. Compared with the null hypothesis that IC_{50} would be unchanged by LKB1 status, ANOVA showed a significant difference in dose-response curve ($P = 7.44E-11$). H358 cells with LKB1 WT or LKB1 KO via CRISPR were treated with azacytidine for 7 days; viability data at the end of the experiment was fitted to a log-logistic model using the *drc* package in R. Compared with the null hypothesis that IC_{50} would be unchanged by LKB1 status, ANOVA showed a significant difference in dose-response curve ($P = 1.37E-09$). **D,** Relative RNA expression of *CXCL8, IRF3, IRF7,* and *TLR2* was determined using RT-PCR. Samples were run in triplicate with analysis by one-way ANOVA with Tukey correction for multiple comparisons. *, $P \leq 0.05$; **, $P \leq 0.01$; ***, $P \leq 0.001$; ****, $P \leq 0.0001$; n.s., nonsignificant.

LKB1 loss associated with decreased sensitivity to azacytidine and paradoxical expression of dsRNA interferon response elements

Based on our observation that repetitive element methylation is decreased and expression is increased in LKB1-loss tumors, we hypothesized that sensitivity to DNMTi treatment with azacytidine would be altered as well. To test this, A549 cells with LKB1 overexpression and H358 cells with LKB1 knockout were treated with azacytidine for 7 days, and cell viability at the end of treatment showed that expression of LKB1 was associated with significantly increased azacytidine sensitivity in both cell lines (**Fig. 3C**). We observed that the effect of cisplatin treatment following azacytidine appeared to be similarly additive in both LKB1-loss and LKB1-overexpressing A549 cells (Supplementary Fig. S9). LKB1 overexpression in A549 cells led to decreased expression of dsRNA response elements such as IRF3, IRF7, and CXCL8. Paradoxically, exposure to azacytidine led to a more robust increase in dsRNA response element expression in the azacytidine-resistant LKB1-loss cells (**Fig. 3D**). This suggests that azacytidine resistance in LKB1 loss is independent of RE transcription, dsRNA sensors, and interferon response elements.

Pioneer transcription factor–binding sites are demethylated in LKB1 loss, and nuclear expression of those factors is LKB1 dependent

CpG demethylation can be induced by the binding of specific transcription factors (TF). To determine if TFs play a role in directing CpG demethylation in LKB1 loss, we explored enrichment of TF consensus binding sites. Using the HOMER algorithm, we determined that hypomethylated sites specific to LKB1 loss are enriched for FOXA, KLF, Nur77, and C/EBP family consensus motifs (**Table 1**; Supplementary Table S3). Analysis of RNA-seq data from the LUAD cohort shows that expression of FOXA1, FOXA3, KLF5, C/EBPβ, and Nur77 is elevated in LKB1-loss tumors (**Fig. 4A**). Furthermore, LKB1-loss–specific hypomethylated CpGs are enriched for FOXA1 and C/EBPβ binding in A549 cells (Supplementary Table S9). These results are consistent with the FOXA family function as "pioneering" TFs that bind to methylated sites and mediate demethylation as well as subsequent transcription (42). KLF5 and C/EBPβ are also suggested to function as pioneering factors (43, 44) and have yet to be associated with LKB1 function in cancer.

Nuclear expression is an important regulating factor for FOXA1, while both expression and nuclear export are important regulating factor for FOXA2 and FOXA3 (42). Overexpression of LKB1 led to decreased total FOXA1 and FOXA2 expression, but no changes in FOXA3 were observed (**Fig. 4B**; Supplementary Fig. S10A). FOXA acetylation, which has been shown to increase stability and FOXA-mediated transcription (45), was reversed as well (**Fig. 4B**). Cellular

fractionation showed that FOXA1 and FOXA3 chromatin binding is attenuated following LKB1 overexpression (**Fig. 4C**; Supplementary Fig. S10B). LKB1 overexpression in LKB1-mutant A549 cells resulted in attenuated nuclear expression of FOXA1 by microscopy as well (**Fig. 4D** and **E**). LKB1-loss A549 cells show reduced viability to FOXA1 silencing compared to LKB1-overexpressing cells (Supplementary Fig. S10C), suggesting that FOXA1 may promote cell survival in LKB1-loss. LKB1 addback in H23 cells and LKB1 knockout in H358 cells resulted in a similar pattern of attenuated nuclear expression of FOXA1 (Supplementary Fig. S11A–S11E).

Like FOXA, C/EBPβ localization in A549 and H23 cell lines is LKB1-dependent and overexpression of LKB1 leads to a reduction in the amount of C/EBPβ bound to chromatin (Supplementary Fig. S12A and S12B). Furthermore, we observed that nuclear expression of C/EBPβ is restored in LKB1-WT states by addition of PI3K/mTOR inhibitor GSK 2126458, suggesting that activation of this pathway by LKB1 loss-of-function is responsible for increased nuclear C/EBPβ expression (Supplementary Fig. S13A–S13D).

Discussion

Our study shows that LKB1 loss in human lung adenocarcinoma results in global CpG demethylation, decreased SAM-e metabolism, repetitive element demethylation, altered FOXA expression and localization, and azacytidine resistance. Taken together, these results suggest that LKB1 loss results in an epigenetic shift driven by altered ability of the cell to maintain CpG methylation and altered activity of pioneering transcription factors. This shift likely plays a significant role in the altered sensitivity to epigenetic therapy we observed.

The literature describes a pattern of hypermethylation in KRAS-mutant lung cancers (8, 21, 38, 39). Research in pancreatic cancer mouse models has suggested that LKB1 loss in KRAS mutant cancers promotes retrotransposon hypermethylation, elevated serine biogenesis (including SAM-e), and enriched DNMT expression (21). In contrast, our observations here show that LKB1 is associated with the opposite phenotype in human lung tumors. We observed that LKB1 loss—regardless of KRAS status—is associated with a pattern of global hypomethylation and downregulation of DNMT1 expression in human lung tumors. Furthermore, we observed that SAM-e levels are lower in LKB1-loss tumors and that TINATs are hypomethylated in LKB1 loss. We hypothesize that depletion of SAM-e is related to altered utilization of methyl donors by alternative enzymes such as NNMT. NNMT overexpression has been directly linked to increased 1-methyl nicotinamide, decreased SAM-e, and altered epigenetic regulation in several cancers, including lung (41). Furthermore, the existing literature arguing for CpG hypermethylation and broad epigenetic repression in KL tumors are based on genetically engineered pancreatic cancer mouse models with a limited set of driver mutations. These

Table 1. TF binding site enrichment of top 5,000 hypomethylated loci.

Rank	Motif	P	% of Targets	% of Backgrounds	Match source
1	TGTTTACTCA	1e-85	18.60%	9.41%	Foxa2 ChIP-seq (GSE25694)
2	GCCACGCCCT	1e-54	11.20%	5.42%	KLF5 ChIP-seq (GSE49402)
3	TTAAAGGTCA	1e-51	4.89%	1.54%	Nur77 ChIP-seq (GSE31363)
4	ATTGCGTAAC	1e-31	13.38%	8.30%	C/EBPβ (Jaspar)
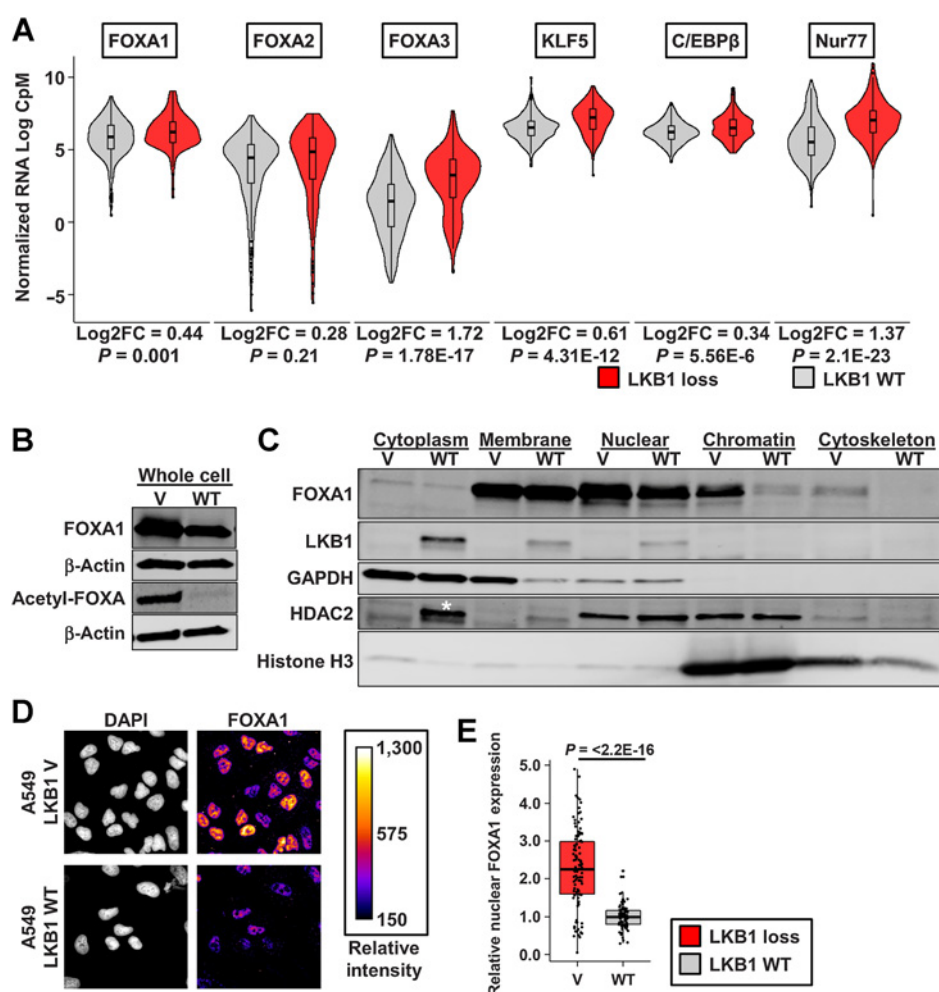
Figure 4.
Hypomethylated CpGs are enriched for FOXA consensus binding sites and LKB1 expression causes transcription factor expression and localization changes. **A,** Normalized Log CpM obtained from limma-voom were obtained for the relavent transcription factors. LogFC and Benjamini-Hochberg adjusted P values obtained using the limma-voom package. **B,** FOXA1 and acetyl-FOXA protein expression was characterized by Western blot in LKB1-deficient A549 cells transfected with pBABE empty vector (V) or pBABE-LKB1 (WT). **C,** A549 cells treated with pBABE-vector (V) or pBABE-LKB1 (WT) were subsequently fractionated to assess FOXA1 expression in the nuclear cytosol or chromatin-bound states. *, this signal is from the previous blot for LKB1, which is approximately the same size of HDAC2. **D,** Nuclear localization of FOXA1 was analyzed by IF microscopy in A549 cells treated with pBABE-vector (V) or pBABE-LKB1 (WT) and is shown to be LKB1-dependent. **E,** Relative nuclear pixel intensity was calculated for A549 cells treated with pBABE-vector (V) or pBABE-LKB1 (WT) and compared using Student t test.

models develop spontaneous, aggressive metastatic disease that likely does not undergo the lengthy, energetically stressed evolution of tumors sequenced in TCGA. Our observations suggest that human LKB1-loss lung cancers undergo a fundamentally different change in metabolite availability and epigenetic remodelling compared to mouse models.

There are several limitations to our study. With regards to histone marks, our comparisons using ENCODE data used NHLF for comparison because of the limited availability of human bronchial epithelial cell (HBEC) histone mark data. HBECs are more similar to the airway epithelial cell precursors that give rise to lung adenocarcinoma, while NHLF are a stromal cell type. Another important limitation is that we did not conclusively determine a mechanism for reduced DNMT1 expression, reduced SAM-e availability in LUAD, and increased chromatin binding of FOXA1. While the observations presented here provide clear evidence that these changes are occurring, future studies will further address these processes.

Our results have broad implications for the study of gene regulation in LKB1-loss lung tumors. Specifically, it appears that there are both global and transcription factor–specific epigenetic alterations in LKB1-loss tumors. The association of LKB1 loss with global demethylation suggests that therapeutics targeting methylation such as azacytidine may have different effects on LKB1-loss and LKB1-WT tumors, as observed *in vitro* here. Importantly, these epigenetic changes are associated with functional LKB1 loss, rather than sequenced mutations alone. Epigenetic modifiers are being actively explored in combination with immunotherapy, and differential effects may be observed in these two classes of lung cancers. In the future, these results should shape patient selection for clinical trials using epigenetic therapy alone or in combination with immunotherapy.

Authors' Disclosures

Authors' Contributions

M.J. Koenig: Conceptualization, data curation, software, formal analysis, validation, investigation, visualization, methodology, writing–original draft, writing–review and editing. **B.A. Agana:** Conceptualization, data curation, formal analysis, investigation, methodology, writing–review and editing. **J.M. Kaufman:** Conceptualization, resources, data curation, software, formal analysis, investigation, visualization, methodology, writing–review and editing. **M.F. Sharpnack:** Data curation, formal analysis, investigation, visualization, writing–review and editing. **W.Z. Wang:** Formal analysis, investigation, writing–review and editing. **C. Weigel:** Formal analysis, investigation, writing–review and editing.

References

1. Han D, Li S-J, Zhu Y-T, Liu L, Li M-X. LKB1/AMPK/mTOR signaling pathway in non-small-cell lung cancer. Asian Pac J Cancer Prev 2013;14:4033–9.
2. Herrmann JL, Byekova Y, Elmets CA, Athar M. Liver kinase B1 (LKB1) in the pathogenesis of epithelial cancers. Cancer Lett 2011;306:1–9.
3. Gao Y, Ge G, Ji H. LKB1 in lung cancerigenesis: a serine/threonine kinase as tumor suppressor. Protein Cell 2011;2:99–107.
4. Ji H, Ramsey MR, Hayes DN, Fan C, McNamara K, Kozlowski P, et al. LKB1 modulates lung cancer differentiation and metastasis. Nature 2007;448:807–10.
5. Marcus AI, Zhou W. LKB1 regulated pathways in lung cancer invasion and metastasis. J Thorac Oncol 2010;5:1883–6.
6. Sanchez-Cespedes M, Parrella P, Esteller M, Nomoto S, Trink B, Engles JM, et al. Inactivation of LKB1/STK11 is a common event in adenocarcinomas of the lung. Cancer Res 2002;62:3659–62.
7. Ding L, Getz G, Wheeler DA, Mardis ER, McLellan MD, Cibulskis K, et al. Somatic mutations affect key pathways in lung adenocarcinoma. Nature 2008; 455:1069–75.
8. Collisson EA, Campbell JD, Brooks AN, Berger AH, Lee W, Chmielecki J, et al. Comprehensive molecular profiling of lung adenocarcinoma. Nature 2014;511: 543–50.
9. Alessi DR, Sakamoto K, Bayascas JR. LKB1-dependent signaling pathways. Annu Rev Biochem 2006;75:137–63.
10. Hezel AF, Bardeesy N. LKB1; linking cell structure and tumor suppression. Oncogene 2008;27:6908–19.
11. Shackelford DB, Shaw RJ. The LKB1-AMPK pathway: metabolism and growth control in tumour suppression. Nat Rev Cancer 2009;9:563–75.
12. Skoulidis F, Hellmann MD, Awad MM, Rizvi H, Carter BW, Denning W, et al. STK11/LKB1 co-mutations to predict for de novo resistance to PD-1/PD-L1 axis blockade in KRAS-mutant lung adenocarcinoma. J Clin Oncol 2017;35:9016.
13. Skoulidis F. STK11/LKB1 Loss of function genomic alterations predict primary resistance to PD-1/PD-L1 axis blockade in KRAS-mutant NSCLC. Paper presented at: World Conference on Lung Cancer; 10/16/2017, 2017; Yokohama Japan.
14. Kaufman JM, Amann JM, Park K, Arasada RR, Li H, Shyr Y, et al. LKB1 Loss induces characteristic patterns of gene expression in human tumors associated with NRF2 activation and attenuation of PI3K-AKT. J Thorac Oncol 2014;9: 794–804.
15. Robertson KD, Ait-Si-Ali S, Yokochi T, Wade PA, Jones PL, Wolffe AP. DNMT1 forms a complex with Rb, E2F1 and HDAC1 and represses transcription from E2F-responsive promoters. Nat Genet 2000;25:338–42.
16. Novakovic B, Wong NC, Sibson M, Ng H-K, Morley R, Manuelpillai U, et al. DNA methylation-mediated down-regulation of DNA methyltransferase-1 (DNMT1) is coincident with, but not essential for, global hypomethylation in human placenta. J Biol Chem 2010;285:9583–93.
17. Okano M, Bell DW, Haber DA, Li E. DNA methyltransferases Dnmt3a and Dnmt3b are essential for de novo methylation and mammalian development. Cell 1999;99:247–57.
18. Kim GD, Ni J, Kelesoglu N, Roberts RJ, Pradhan S. Co-operation and communication between the human maintenance and de novo DNA (cytosine-5) methyltransferases. EMBO J 2002;21:4183–95.
19. Detich N, Hamm S, Just G, Knox JD, Szyf M. The methyl donor S-adenosylmethionine inhibits active demethylation of DNA: a candidate novel mechanism for the pharmacological effects of S-adenosylmethionine. J Biol Chem 2003;278:20812–20.
20. Chiang PK, Gordon RK, Tal J, Zeng GC, Doctor BP, Pardhasaradhi K, et al. S-Adenosylmethionine and methylation. FASEB J 1996;10:471–80.
21. Kottakis F, Nicolay BN, Roumane A, Karnik R, Gu H, Nagle JM, et al. LKB1 loss links serine metabolism to DNA methylation and tumorigenesis. Nature 2016; 539:390–5.
22. Stresemann C, Lyko F. Modes of action of the DNA methyltransferase inhibitors azacytidine and decitabine. Int J Cancer 2008;123:8–13.
23. Kitajima S, Ivanova E, Guo S, Yoshida R, Campisi M, Sundararaman SK, et al. Suppression of STING associated with LKB1 loss in KRAS-driven lung cancer. Cancer Discov 2018;9:34–45.
24. Zhang H, Fillmore Brainson C, Koyama S, Redig AJ, Chen T, Li S, et al. Lkb1 inactivation drives lung cancer lineage switching governed by Polycomb Repressive Complex 2. Nat Commun 2017;8:14922.
25. Brocks D, Schmidt CR, Daskalakis M, Jang HS, Shah NM, Li D, et al. DNMT and HDAC inhibitors induce cryptic transcription start sites encoded in long terminal repeats. Nat Genet 2017;49:1052.
26. Chiappinelli Katherine B, Strissel Pamela L, Desrichard A, Li H, Henke C, Akman B, et al. Inhibiting DNA methylation causes an interferon response in cancer via dsRNA including endogenous retroviruses. Cell 2015;162:974–86.
27. Roulois D, Loo Yau H, Singhania R, Wang Y, Danesh A, Shen SY, et al. DNA-demethylating agents target colorectal cancer cells by inducing viral mimicry by endogenous transcripts. Cell 2015;162:961–73.
28. Du P, Zhang X, Huang C-C, Jafari N, Kibbe WA, Hou L, et al. Comparison of Beta-value and M-value methods for quantifying methylation levels by microarray analysis. BMC Bioinformatics 2010;11:587.
29. Wilhelm-Benartzi CS, Koestler DC, Karagas MR, Flanagan JM, Christensen BC, Kelsey KT, et al. Review of processing and analysis methods for DNA methylation array data. Br J Cancer 2013;109:1394–402.
30. Heinz S, Benner C, Spann N, Bertolino E, Lin YC, Laslo P, et al. Simple combinations of lineage-determining transcription factors prime cis-regulatory elements required for macrophage and B cell identities. Mol Cell 2010;38:576–89.
31. Navarro FC, Hoops J, Bellfy L, Cerveira E, Zhu Q, Zhang C, et al. TeXP: deconvolving the effects of pervasive and autonomous transcription of transposable elements. PLoS Comput Biol 2019;15:e1007293.
32. Kaufman JM, Yamada T, Park K, Timmers CD, Amann JM, Carbone DP. A transcriptional signature identifies LKB1 functional status as a novel determinant of MEK sensitivity in lung adenocarcinoma. Cancer Res 2017; 77:153–63.
33. Ran FA, Hsu PD, Wright J, Agarwala V, Scott DA, Zhang F. Genome engineering using the CRISPR-Cas9 system. Nat Protoc 2013;8:2281–308.
34. Huang L-K, Wang M-JJ. Image thresholding by minimizing the measures of fuzziness. Pattern Recognit 1995;28:41–51.
35. Ehrich M, Nelson MR, Stanssens P, Zabeau M, Liloglou T, Xinarianos G, et al. Quantitative high-throughput analysis of DNA methylation patterns

by base-specific cleavage and mass spectrometry. Proc Natl Acad Sci U S A 2005; 102:15785–90.

36. Li S, Park Y, Duraisingham S, Strobel FH, Khan N, Soltow QA, et al. Predicting network activity from high throughput metabolomics. PLoS Comput Biol 2013; 9:e1003123.

37. Vidal E, Sayols S, Moran S, Guillaumet-Adkins A, Schroeder MP, Royo R, et al. A DNA methylation map of human cancer at single base-pair resolution. Oncogene 2017;36:5648–57.

38. Selamat SA, Chung BS, Girard L, Zhang W, Zhang Y, Campan M, et al. Genome-scale analysis of DNA methylation in lung adenocarcinoma and integration with mRNA expression. Genome Res 2012;22:1197–211.

39. Toyooka S, Tokumo M, Shigematsu H, Matsuo K, Asano H, Tomii K, et al. Mutational and epigenetic evidence for independent pathways for lung adenocarcinomas arising in smokers and never smokers. Cancer Res 2006;66: 1371–5.

40. Ogino S, Kawasaki T, Kirkner GJ, Loda M, Fuchs CS. CpG island methylator phenotype-low (CIMP-low) in colorectal cancer: possible associations with male sex and KRAS mutations. J Mol Diagn 2006;8: 582–8.

41. Ulanovskaya OA, Zuhl AM, Cravatt BF. NNMT promotes epigenetic remo-deling in cancer by creating a metabolic methylation sink. Nat Chem Biol 2013;9:300–6.

42. Lam EW, Brosens JJ, Gomes AR, Koo CY. Forkhead box proteins: tuning forks for transcriptional harmony. Nat Rev Cancer 2013;13:482–95.

43. Diakiw SM, D'Andrea RJ, Brown AL. The double life of KLF5: opposing roles in regulation of gene-expression, cellular function, and transformation. IUBMB Life 2013;65:999–1011.

44. Wang F, Demura M, Cheng Y, Zhu A, Karashima S, Yoneda T, et al. Dynamic CCAAT/enhancer binding protein-associated changes of DNA methylation in the angiotensinogen gene. Hypertension 2014;63: 281–8.

45. van Gent R, Di Sanza C, van den Broek NJF, Fleskens V, Veenstra A, Stout GJ, et al. SIRT1 mediates FOXA2 breakdown by deacetylation in a nutrient-dependent manner. PLoS One 2014;9:e98438.